

Chapter 10

Stimulated Raman Scattering and Stimulated Rayleigh-Wing Scattering

10.1 The Spontaneous Raman Effect

The spontaneous Raman effect was discovered by C.V. Raman in 1928. To observe this effect, a beam of light illuminates a material sample (which can be a solid, liquid, or gas), and the scattered light is observed spectroscopically, as illustrated in Fig. 10.1.1. In general, the scattered light contains frequencies different from those of the excitation source. Those new components shifted to lower frequencies are called Stokes components, and those shifted to higher frequencies are called anti-Stokes components. The Stokes components are typically orders of magnitude more intense than the anti-Stokes components.

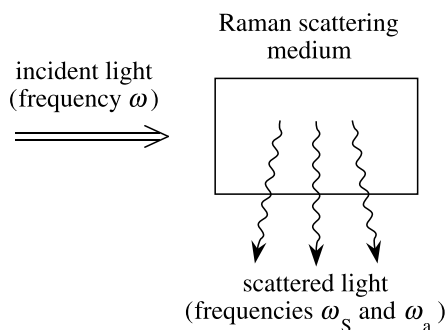


FIGURE 10.1.1: Spontaneous Raman scattering.

These properties of Raman scattering can be understood through use of the energy level diagrams shown in Fig. 10.1.2. Raman Stokes scattering consists of a transition from the ground state g to the final state n by means of a virtual intermediate level associated with excited state n' . Raman anti-Stokes scattering entails a transition from level n to level g with n' serving

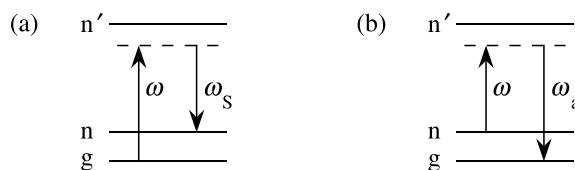


FIGURE 10.1.2: Energy level diagrams describing (a) Raman Stokes scattering and (b) Raman anti-Stokes scattering.

as the intermediate level. The anti-Stokes lines are typically much weaker than the Stokes lines because, in thermal equilibrium, the population of level n is smaller than the population in level g by the Boltzmann factor $\exp(-\hbar\omega_{ng}/kT)$.

The Raman effect has important spectroscopic applications because transitions that are one-photon forbidden can often be studied using Raman scattering. For example, the Raman transitions illustrated in Fig. 10.1.2 can occur only if the matrix elements $\langle g|\hat{\mathbf{r}}|n'\rangle$ and $\langle n'|\hat{\mathbf{r}}|n\rangle$ are both nonzero, and this fact implies (for a material system that possesses inversion symmetry, so that the energy eigenstates possess definite parity) that the states g and n must possess the same parity. But under these conditions the $g \rightarrow n$ transition is forbidden for single-photon electric dipole transitions because the matrix element $\langle g|\hat{\mathbf{r}}|n\rangle$ must necessarily vanish.

10.2 Spontaneous versus Stimulated Raman Scattering

The spontaneous Raman scattering process described in the previous section is typically a rather weak process. Even for condensed matter, the scattering cross section per unit volume for Raman Stokes scattering is only approximately 10^{-6} cm^{-1} . Hence, in propagating through 1 cm of the scattering medium, only approximately 1 part in 10^6 of the incident radiation will be scattered into the Stokes frequency.

However, under excitation by an intense laser beam, highly efficient scattering can occur as a result of the stimulated version of the Raman scattering process. Stimulated Raman scattering is typically a very strong scattering process: 10% or more of the energy of the incident laser beam is often converted into the Stokes frequency. Another difference between spontaneous and stimulated Raman scattering is that the spontaneous process leads to emission in the form of a dipole radiation pattern, whereas the stimulated process leads to emission in a narrow cone in the forward and backward directions. Stimulated Raman scattering was discovered by Woodbury and Ng (1962) and was described more fully by Eckhardt et al. (1962). The properties of stimulated Raman scattering have been reviewed by Shen and Bloembergen (1965), Bloembergen (1967), Kaiser and Maier (1972), Penzkofer et al. (1979), and Raymer and Walmsley (1990).

The relation between spontaneous and stimulated Raman scattering can be understood in terms of an argument (Hellwarth, 1963) that considers the process from the point of view of the photon occupation numbers of the various field modes. One postulates that the probability per unit time that a photon will be emitted into Stokes mode S is given by

$$P_S = Dm_L(m_S + 1). \quad (10.2.1)$$

Here m_L is the mean number of photons per mode in the laser radiation, m_S is the mean number of photons in Stokes mode S , and D is a proportionality constant whose value depends on the physical properties of the material medium. This functional form is assumed because the factor m_L leads to the expected linear dependence of the transition rate on the laser intensity, and the factor $m_S + 1$ leads to stimulated scattering through the contribution m_S and to spontaneous scattering through the contribution of unity. This dependence on the factor $m_S + 1$ is reminiscent of the stimulated and spontaneous contributions to the total emission rate for a single-photon transition of an atomic system as treated by the Einstein A and B coefficients. Eq. (10.2.1) can be justified by more rigorous treatments; note, for example, that the results of the present analysis are consistent with those of the fully quantum-mechanical treatment of Raymer and Mostowski (1981).

By the definition of P_S as a probability per unit time for emitting a photon into mode S , the time rate of change of the mean photon occupation number for the Stokes mode is given by $dm_S/dt = P_S$ or through the use of Eq. (10.2.1) by

$$\frac{dm_S}{dt} = Dm_L(m_S + 1). \quad (10.2.2)$$

If we now assume that the Stokes mode corresponds to a wave traveling in the positive z direction at the velocity c/n , as illustrated in Fig. 10.2.1, we see that the time rate of change given by Eq. (10.2.2) corresponds to a spatial growth rate given by

$$\frac{dm_S}{dz} = \frac{1}{c/n} \frac{dm_S}{dt} = \frac{1}{c/n} Dm_L(m_S + 1). \quad (10.2.3)$$

For definiteness, Fig. 10.2.1 shows the laser and Stokes beams propagating in the same direction; in fact, Eq. (10.2.3) applies even if the angle between the propagation directions of the laser and Stokes waves is arbitrary, as long as z is measured along the propagation direction of the Stokes wave.

It is instructive to consider Eq. (10.2.3) in the two opposite limits of $m_S \ll 1$ and $m_S \gg 1$. In the first limit, where the occupation number of the Stokes mode is much less than unity, Eq. (10.2.3) becomes simply

$$\frac{dm_S}{dz} = \frac{1}{c/n} Dm_L \quad (\text{for } m_S \ll 1). \quad (10.2.4)$$

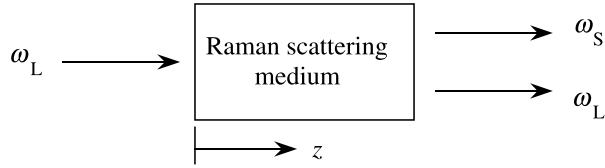


FIGURE 10.2.1: Geometry describing stimulated Raman scattering.

The solution to this equation for the geometry of Fig. 10.2.1 under the assumption that the laser field is unaffected by the interaction (and thus that m_L is independent of z) is

$$m_S(z) = m_S(0) + \frac{1}{c/n} D m_L z \quad (\text{for } m_S \ll 1), \quad (10.2.5)$$

where $m_S(0)$ denotes the photon occupation number associated with the Stokes field at the input to the Raman medium. This limit corresponds to spontaneous Raman scattering; the Stokes intensity increases in proportion to the length of the Raman medium and thus to the total number of molecules contained in the interaction region.

The opposite limiting case is that in which there are many photons in the Stokes mode. In this case Eq. (10.2.3) becomes

$$\frac{dm_S}{dz} = \frac{1}{c/n} D m_L m_S \quad (\text{for } m_S \gg 1), \quad (10.2.6)$$

whose solution (again under the assumption of an undepleted input field) is

$$m_S(z) = m_S(0) e^{Gz} \quad (\text{for } m_S \gg 1), \quad (10.2.7)$$

where we have introduced the Raman gain coefficient

$$G = \frac{D m_L}{c/n}. \quad (10.2.8)$$

Again $m_S(0)$ denotes the photon occupation number associated with the Stokes field at the input to the Raman medium. If no field is injected into the Raman medium, $m_S(0)$ represents the quantum noise associated with the vacuum state, which is equivalent to one photon per mode. Emission of the sort described by Eq. (10.2.7) is called stimulated Raman scattering. The Stokes intensity is seen to grow exponentially with propagation distance through the medium, and large values of the Stokes intensity are routinely observed at the output of the interaction region.

We see from Eq. (10.2.8) that the Raman gain coefficient can be related simply to the phenomenological constant D introduced in Eq. (10.2.1). However, we see from Eq. (10.2.5) that the strength of spontaneous Raman scattering is also proportional to D . Since the strength of

spontaneous Raman scattering is often described in terms of a scattering cross section, it is thus possible to determine a relationship between the gain coefficient G for stimulated Raman scattering and the cross section for spontaneous Raman scattering. This relationship is derived as follows.

Since one laser photon is lost for each Stokes photon that is created, the occupation number of the laser field changes as the result of spontaneous scattering into one particular Stokes mode in accordance with the relation $dm_L/dz = -dm_S/dz$, with dm_S/dz given by Eq. (10.2.4). However, since the system can radiate into a large number of Stokes modes, the total rate of loss of laser photons is given by

$$\frac{dm_L}{dz} = -Mb \frac{dm_S}{dz} = \frac{-Dm_L Mb}{c/n}, \quad (10.2.9)$$

where M is the total number of modes into which the system can radiate and where b is a geometrical factor that accounts for the fact that the angular distribution of scattered radiation may be nonuniform and hence that the scattering rate into different Stokes modes may be different. Explicitly, b is the ratio of the angularly averaged Stokes emission rate to the rate in the direction of the particular Stokes mode S for which D (and thus the Raman gain coefficient) is to be determined. If $|f(\theta, \phi)|^2$ denotes the angular distribution of the Stokes radiation, b is then given by

$$b = \frac{\int |f(\theta, \phi)|^2 d\Omega/4\pi}{|f(\theta_S, \phi_S)|^2}, \quad (10.2.10)$$

where (θ_S, ϕ_S) gives the direction of the particular Stokes mode for which D is to be determined.

The total number of Stokes modes into which the system can radiate is given by the expression (see, for example, Boyd, 1983, Eq. (3.4.4))

$$M = \frac{V \omega_S^2 \Delta\omega}{\pi^2 (c/n)^3}, \quad (10.2.11)$$

where V denotes the volume of the region in which the modes are defined and where $\Delta\omega$ denotes the linewidth of the scattered Stokes radiation. The rate of loss of laser photons is conventionally described by the cross section σ for Raman scattering, which is defined by the relation

$$\frac{dm_L}{dz} = -N\sigma m_L, \quad (10.2.12)$$

where N is the number density of molecules. By comparison of Eqs. (10.2.9) and (10.2.12), we see that we can express the parameter D in terms of the cross section σ by

$$D = \frac{N\sigma (c/n)}{Mb}. \quad (10.2.13)$$

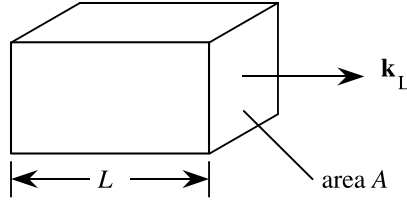


FIGURE 10.2.2: Geometry of the region within which the laser and Stokes modes are defined.

This expression for D , with M given by Eq. (10.2.11), is now substituted into expression (10.2.8) for the Raman gain coefficient to give the result

$$G = \frac{N\sigma\pi^2c^3m_L}{V\omega_S^2\Delta\omega bn^3} \equiv \frac{N\pi^2c^3m_L}{V\omega_S^2bn^3} \left(\frac{\partial\sigma}{\partial\omega} \right)_0, \quad (10.2.14)$$

where in obtaining the second form we have used the definition of the spectral density of the scattering cross section to express σ in terms of its line-center value $(\partial\sigma/\partial\omega)_0$ as

$$\sigma = \left(\frac{\partial\sigma}{\partial\omega} \right)_0 \Delta\omega. \quad (10.2.15)$$

Eq. (10.2.14) gives the Raman gain coefficient in terms of the number of laser photons per mode, m_L . In order to express the gain coefficient in terms of the laser intensity, which can be measured directly, we assume the geometry shown in Fig. 10.2.2. The laser intensity I_L is equal to the number of photons contained in this region multiplied by the energy per photon and divided by the cross-sectional area of the region and by the transit time through the region—that is,

$$I_L = \frac{m_L\hbar\omega_L}{A(nL/c)} = \frac{m_L\hbar\omega_Lc}{Vn}, \quad (10.2.16)$$

where $V = AL$. Through use of this result, the Raman gain coefficient of Eq. (10.2.14) can be expressed as

$$G = \frac{N\pi^2c^2}{\omega_S^2bn^2\hbar\omega_L} \left(\frac{\partial\sigma}{\partial\omega} \right)_0 I_L. \quad (10.2.17)$$

It is sometimes convenient to express the Raman gain coefficient not in terms of the spectral cross section $(\partial\sigma/\partial\omega)_0$ but in terms of the differential spectral cross section $(\partial^2\sigma/\partial\omega\partial\Omega)_0$, where $d\Omega$ is an element of solid angle. These quantities are related by

$$\left(\frac{\partial\sigma}{\partial\omega} \right)_0 = 4\pi b \left(\frac{\partial^2\sigma}{\partial\omega\partial\Omega} \right)_0, \quad (10.2.18)$$

where b is the factor defined in Eq. (10.2.10) that accounts for the possible nonuniform angular distribution of the scattered Stokes radiation. Through use of this relation, Eq. (10.2.17)

TABLE 10.2.1: Properties of stimulated Raman scattering for several materials^a.

Substance	Frequency shift ν_0 (cm ⁻¹)	Linewidth $\Delta\nu$ (cm ⁻¹)	Cross section $N(d\sigma/d\Omega)_0$ (10 ⁻⁶ m ⁻¹ sr ⁻¹)	Gain factor ^b G/I_L (m/TW)
Liquid O ₂	1552	0.117	0.48 ± 0.14	145 ± 40
Liquid N ₂	2326.5	0.067	0.29 ± 0.09	160 ± 50
Benzene	992	2.15	3.06	28
CS ₂	655.6	0.50	7.55	240
Nitrobenzene	1345	6.6	6.4	21
Bromobenzene	1000	1.9	1.5	15
Chlorobenzene	1002	1.6	1.5	19
Toluene	1003	1.94	1.1	12
NiNbO ₃	256	23	381	89
	637	20	231	94
Ba ₂ NaNb ₅ O ₁₅	650			67
LiTaO ₃	201	22	238	44
SiO ₂	467			08
Methane gas	2916		(10 atm) ^c	6.6
H ₂ gas	4155		(> 10 atm)	15
H ₂ gas (rotat.)	450		(> 0.5 atm)	5
Deuterium gas	2991		(> 10 atm)	11
N ₂ gas	2326		(10 atm) ^c	0.71
O ₂ gas	1555		(10 atm) ^c	0.16

^a After Kaiser and Maier (1972) and Simon and Tittel (1994). All transitions are vibrational except for the 450 cm⁻¹ hydrogen transition which is rotational.

^b Measured at 694 nm unless stated otherwise.

^c Measured at 500 nm.

becomes

$$G = \frac{4\pi^3 N c^2}{\omega_S^2 \hbar \omega_L n_S^2} \left(\frac{\partial^2 \sigma}{\partial \omega \partial \Omega} \right)_0 I_L. \quad (10.2.19)$$

Some of the parameters describing stimulated Raman scattering are listed in Table 10.2.1 for a number of materials.

10.3 Stimulated Raman Scattering Described by the Nonlinear Polarization

Here we develop a classical (that is, non-quantum-mechanical) model that describes stimulated Raman scattering (see also Garmire et al., 1963). For conceptual clarity, our treatment is re-

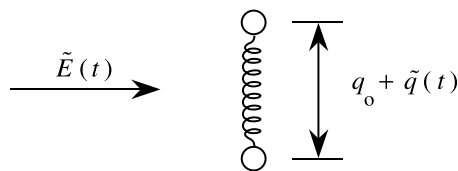


FIGURE 10.3.1: Molecular description of stimulated Raman scattering.

stricted to the scalar approximation. Treatments that include the tensor properties of Raman interaction are cited in the references listed at the end of this chapter.

We assume that the optical field interacts with a vibrational mode of a molecule, as illustrated in Fig. 10.3.1. We assume that the vibrational mode can be described as a simple harmonic oscillator of resonance frequency ω_v and damping constant γ , and we denote by $\tilde{q}(t)$ the deviation of the internuclear distance from its equilibrium value q_0 . The equation of motion describing the molecule vibration is thus

$$\frac{d^2\tilde{q}}{dt^2} + 2\gamma \frac{d\tilde{q}}{dt} + \omega_v^2 \tilde{q} = \frac{\tilde{F}(t)}{m}, \quad (10.3.1)$$

where $\tilde{F}(t)$ denotes any force that acts on the vibrational mode and where m represents the reduced nuclear mass.

The key assumption of the theory is that the optical polarizability of the molecule (which is typically predominantly electronic in origin) is not constant, but depends on the internuclear separation $\tilde{q}(t)$ according to the equation

$$\tilde{\alpha}(t) = \alpha_0 + \left(\frac{\partial \alpha}{\partial q} \right)_0 \tilde{q}(t). \quad (10.3.2)$$

Here α_0 is the polarizability of a molecule in which the internuclear distance is held fixed at its equilibrium value. According to Eq. (10.3.2), when the molecule is set into oscillation its polarizability will be modulated periodically in time, and thus the refractive index of a collection of coherently oscillating molecules will be modulated in time in accordance with the relations

$$\tilde{n}(t) = \sqrt{\tilde{\epsilon}(t)} = [1 + N\tilde{\alpha}(t)]^{1/2}. \quad (10.3.3)$$

The temporal modulation of the refractive index will modify a beam of light as it passes through the medium. In particular, frequency sidebands separated from the laser frequency by $\pm\omega_v$ will be impressed upon the transmitted laser beam.

Next, we examine how molecular vibrations can be driven coherently by an applied optical field. In the presence of the optical field $\tilde{E}(z, t)$, each molecule will become polarized, and the

induced dipole moment of a molecule located at coordinate z will be given by

$$\tilde{\mathbf{p}}(z, t) = \epsilon_0 \alpha \tilde{\mathbf{E}}(z, t). \quad (10.3.4)$$

The energy required to establish this oscillating dipole moment is given by

$$W = \frac{1}{2} \langle \tilde{\mathbf{p}}(z, t) \cdot \tilde{\mathbf{E}}(z, t) \rangle = \frac{1}{2} \epsilon_0 \alpha \langle \tilde{E}^2(z, t) \rangle, \quad (10.3.5)$$

where the angular brackets denote a time average over an optical period. The applied optical field hence exerts a force given by

$$\tilde{F} = \frac{dW}{dq} = \frac{\epsilon_0}{2} \left(\frac{d\alpha}{dq} \right)_0 \langle \tilde{E}^2(z, t) \rangle \quad (10.3.6)$$

on the vibrational degree of freedom. In particular, if the applied field contains two frequency components, Eq. (10.3.6) shows that the vibrational coordinate will experience a time-varying force at the beat frequency between the two field components.

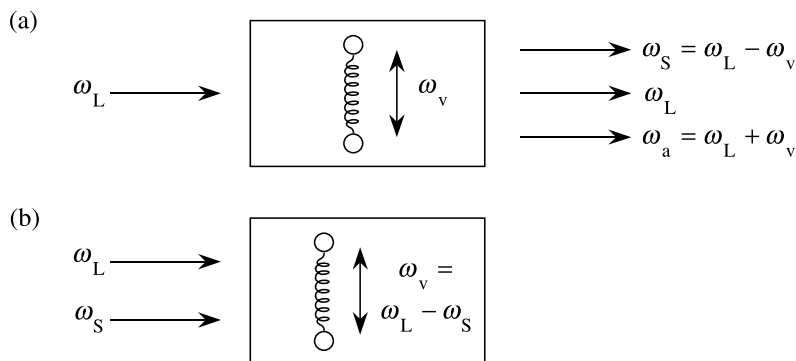


FIGURE 10.3.2: Stimulated Raman scattering. (a) A laser beam at frequency ω_L scatters off a molecule vibrating at frequency ω_v to generate light at the Stokes frequency ω_S and the anti-Stokes frequency ω_a . (b) Light beams at frequencies ω_L and ω_S illuminate a molecule. The beat note between these two frequencies drive a molecular vibration at frequency $\omega_v = \omega_L - \omega_S$.

The origin of stimulated Raman scattering can be understood schematically in terms of the interactions shown in Fig. 10.3.2. Part (a) of the figure shows how molecular vibrations modulate the refractive index of the medium at frequency ω_v and thereby impress frequency sidebands onto the laser field. Part (b) shows how the Stokes field at frequency $\omega_S = \omega_L - \omega_v$ can beat with the laser field to produce a modulation of the total intensity of the form

$$\tilde{I}(t) = I_0 + I_1 \cos[(\omega_L - \omega_S)t + \phi] \quad (10.3.7)$$

where ϕ is some relative phase. This modulated intensity coherently excites the molecular oscillation at frequency $\omega_L - \omega_S = \omega_v$. The two processes shown in parts (a) and (b) of the

figure reinforce one another in the sense that the interaction shown in part (b) leads to a stronger molecular vibration, which by the interaction shown in part (a) leads to a stronger Stokes field, which in turn leads to a stronger molecular vibration.

To make these ideas quantitative, let us assume that the total optical field can be represented as

$$\tilde{E}(z, t) = A_L e^{i(k_L z - \omega_L t)} + A_S e^{i(k_S z - \omega_S t)} + \text{c.c.} \quad (10.3.8)$$

According to Eq. (10.3.6) the time-varying part of the applied force is then given by

$$\tilde{F}(z, t) = \epsilon_0 \left(\frac{\partial \alpha}{\partial q} \right)_0 [A_L A_S^* e^{i(Kz - \Omega t)} + \text{c.c.}], \quad (10.3.9)$$

where we have introduced the notation

$$K = k_L - k_S \quad \text{and} \quad \Omega = \omega_L - \omega_S. \quad (10.3.10)$$

We next find the solution to Eq. (10.3.1) with a force term of the form of Eq. (10.3.9). We adopt a trial solution of the form

$$\tilde{q}(t) = q(\Omega) e^{i(Kz - \Omega t)} + \text{c.c.} \quad (10.3.11)$$

We insert Eqs. (10.3.9) and (10.3.11) into Eq. (10.3.1), which becomes

$$-\Omega^2 q(\Omega) - 2i\Omega\gamma q(\Omega) + \omega_v^2 q(\Omega) = \frac{\epsilon_0}{m} \left(\frac{\partial \alpha}{\partial q} \right)_0 A_L A_S^*,$$

and we thus find that the amplitude of the molecular vibration is given by

$$q(\Omega) = \frac{(\epsilon_0/m)(\partial \alpha / \partial q)_0 A_L A_S^*}{\omega_v^2 - \Omega^2 - 2i\Omega\gamma}. \quad (10.3.12)$$

The polarization of the medium is given according to Eqs. (10.3.2) and (10.3.4) by

$$\begin{aligned} \tilde{P}(z, t) &= N \tilde{p}(z, t) = \epsilon_0 N \tilde{\alpha}(z, t) \tilde{E}(z, t) \\ &= \epsilon_0 N \left[\alpha_0 + \left(\frac{\partial \alpha}{\partial q} \right)_0 \tilde{q}(z, t) \right] \tilde{E}(z, t), \end{aligned} \quad (10.3.13)$$

and consequently the nonlinear part of the polarization is given by

$$\begin{aligned} \tilde{P}^{\text{NL}}(z, t) &= \epsilon_0 N \left(\frac{\partial \alpha}{\partial q} \right)_0 [q(\Omega) e^{i(Kz - \Omega t)} + \text{c.c.}] \\ &\quad \times [A_L e^{i(k_L z - \omega_L t)} + A_S e^{i(k_S z - \omega_S t)} + \text{c.c.}]. \end{aligned} \quad (10.3.14)$$

The nonlinear polarization is thus seen to contain several different frequency components. The part of this expression that oscillates at frequency ω_S is known as the Stokes polarization and is given by

$$\tilde{P}_S^{\text{NL}}(z, t) = P(\omega_S)e^{-i\omega_S t} + \text{c.c.} \quad (10.3.15)$$

with a complex amplitude given by

$$P(\omega_S) = N\epsilon_0 \left(\frac{\partial \alpha}{\partial q} \right)_0 q^*(\Omega) A_L e^{ik_S z}. \quad (10.3.16)$$

By introducing the expression (10.3.12) for $q(\Omega)$ into this equation, we find that the complex amplitude of the Stokes polarization is given by

$$P(\omega_S) = \frac{(\epsilon_0^2 N/m)(\partial \alpha / \partial q)_0^2 |A_L|^2 A_S}{\omega_v^2 - \Omega^2 + 2i\Omega\gamma} e^{ik_S z}. \quad (10.3.17)$$

We now define the Raman susceptibility through the expression

$$P(\omega_S) = 6\epsilon_0 \chi_R(\omega_S) |A_L|^2 A_S e^{ik_S z}, \quad (10.3.18)$$

where for notational convenience we have introduced $\chi_R(\omega_S)$ as a shortened form of $\chi^{(3)}(\omega_S = \omega_S + \omega_L - \omega_L)$. By comparison of Eqs. (10.3.17) and (10.3.18), we find that the Raman susceptibility is given by

$$\chi_R(\omega_S) = \frac{\epsilon_0(N/6m)(\partial \alpha / \partial q)_0^2}{\omega_v^2 - (\omega_L - \omega_S)^2 + 2i(\omega_L - \omega_S)\gamma}. \quad (10.3.19a)$$

The real and imaginary parts of $\chi_R(\omega_S) \equiv \chi'_R(\omega_S) + i\chi''_R(\omega_S)$ are illustrated in Fig. 10.3.3. Near the Raman resonance, the Raman susceptibility can be approximated as

$$\chi_R(\omega_S) = \frac{(\epsilon_0 N/12m\omega_v)(\partial \alpha / \partial q)_0^2}{[\omega_S - (\omega_L - \omega_v)] + i\gamma}. \quad (10.3.19b)$$

Note that, at the exact Raman resonance (that is, for $\omega_S = \omega_L - \omega_v$), the Raman susceptibility is negative imaginary. (We shall see below that consequently the Stokes wave experiences amplification.)

In order to describe explicitly the spatial evolution of the Stokes wave, we use Eqs. (10.3.8), (10.3.15), (10.3.18), and (9.3.19) for the nonlinear polarization appearing in the driven wave equation (2.1.17). We then find that the evolution of the field amplitude A_S is given in the slowly varying amplitude approximation by

$$\frac{dA_S}{dz} = -\alpha_S A_S, \quad (10.3.20)$$

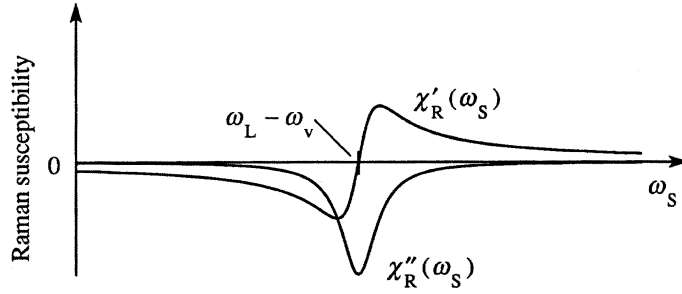


FIGURE 10.3.3: Resonance structure of the Raman susceptibility.

where

$$\alpha_S = -3i \frac{\omega_S}{n_{SC}} \chi_R(\omega_S) |A_L|^2 \quad (10.3.21)$$

is the Stokes wave “absorption” coefficient. Since the imaginary part of $\chi_R(\omega_S)$ is negative, the real part of the absorption coefficient is negative, implying that the Stokes wave actually experiences exponential growth. Note that α_S depends only on the modulus of the complex amplitude of the laser field. Raman Stokes amplification is thus a process for which the phase-matching condition is automatically satisfied. Alternatively, Raman Stokes amplification can be said to be a pure gain process or a nonparametric process.

We can also predict the spatial evolution of a wave at the anti-Stokes frequency through use of the results of the calculation just completed. In the derivation of Eq. (10.3.19a), no assumptions were made regarding the sign of $\omega_L - \omega_S$. We can thus deduce the form of the anti-Stokes susceptibility by formally replacing ω_S by ω_a in Eq. (10.3.19a) to obtain the result

$$\chi_R(\omega_a) = \frac{\epsilon_0(N/6m)(\partial\alpha/\partial q)_0^2}{\omega_v^2 - (\omega_L - \omega_a)^2 + 2i(\omega_L - \omega_a)\gamma}. \quad (10.3.22)$$

Since ω_S and ω_a are related through

$$\omega_L - \omega_S = -(\omega_L - \omega_a), \quad (10.3.23)$$

we see that

$$\chi_R(\omega_a) = \chi_R(\omega_S)^*. \quad (10.3.24)$$

The relation between the Stokes and anti-Stokes Raman susceptibilities is illustrated in Fig. 10.3.4. Near the Raman resonance, Eq. (10.3.22) can be approximated by

$$\chi_R(\omega_a) = \frac{-(\epsilon_0 N/12m\omega_v)(\partial\alpha/\partial q)_0^2}{[\omega_a - (\omega_L + \omega_v)] + i\gamma}, \quad (10.3.25)$$

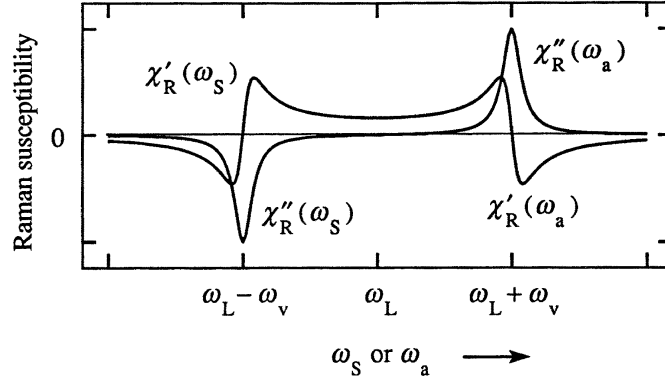


FIGURE 10.3.4: Relation between Stokes and anti-Stokes Raman susceptibilities.

and at the exact resonance the Raman susceptibility is positive imaginary. The amplitude of the anti-Stokes wave hence obeys the propagation equation

$$\frac{dA_a}{dz} = -\alpha_a A_a, \quad (10.3.26)$$

where

$$\alpha_a = -3i \frac{\omega_a}{n_a c} \chi_R(\omega_a) |A_L|^2. \quad (10.3.27)$$

For a positive imaginary $\chi_R(\omega_a)$, α_a is positive real, implying that the anti-Stokes wave experiences attenuation.

However, it was found experimentally (Terhune, 1963) that the anti-Stokes wave is generated with appreciable efficiency in certain directions. The origin of anti-Stokes generation is an additional contribution to the nonlinear polarization beyond that described by the Raman susceptibility of Eq. (10.3.25). Inspection of Eq. (10.3.14) shows that there is a contribution to the anti-Stokes polarization

$$\tilde{P}_a^{\text{NL}}(z, t) = P(\omega_a) e^{-i\omega_a t} + \text{c.c.} \quad (10.3.28)$$

that depends on the Stokes amplitude and which is given by

$$P(\omega_a) = N\epsilon_0 \left(\frac{\partial \alpha}{\partial q} \right)_0 q(\Omega) A_L = \frac{(N\epsilon_0^2/m)(\partial \alpha / \partial q)_0^2 A_L^2 A_S^*}{\omega_v^2 - \Omega^2 - 2i\Omega\gamma} e^{i(2k_L - k_S)z}. \quad (10.3.29)$$

(Recall that $\Omega \equiv \omega_L - \omega_S = \omega_a - \omega_L$.) This contribution to the nonlinear polarization can be described in terms of a four-wave mixing susceptibility $\chi_F(\omega_a) \equiv \chi^{(3)}(\omega_a = \omega_L + \omega_L - \omega_S)$, which is defined by the relation

$$P(\omega_a) = 3\epsilon_0 \chi_F(\omega_a) A_L^2 A_S^* e^{i(2k_L - k_S)z}, \quad (10.3.30)$$

and which is hence equal to

$$\chi_F(\omega_a) = \frac{(N\epsilon_0/3m)(\partial\alpha/\partial q)_0^2}{\omega_v^2 - (\omega_L - \omega_a)^2 + 2i(\omega_L - \omega_a)\gamma}. \quad (10.3.31)$$

We can see by comparison with Eq. (10.3.22) that

$$\chi_F(\omega_a) = 2\chi_R(\omega_a). \quad (10.3.32)$$

The total polarization at the anti-Stokes frequency is the sum of the contributions described by Eqs. (10.3.22) and (10.3.31) and is thus given by

$$P(\omega_a) = 6\epsilon_0\chi_R(\omega_a)|A_L|^2 A_a e^{ik_a z} + 3\epsilon_0\chi_F(\omega_a)A_L^2 A_S^* e^{i(2k_L - k_s)z}. \quad (10.3.33)$$

The first term in this expression is automatically phase matched (see also the discussion following Eq. (10.3.21)) and describes a nonparametric process. The second term is not automatically phase matched and describes the parametric process of four-wave mixing.

Similarly, there is a four-wave mixing contribution to the Stokes polarization described by

$$\chi_F(\omega_S) = \frac{(N\epsilon_0/3m)(\partial\alpha/\partial q)_0^2}{\omega_v^2 - (\omega_L - \omega_S)^2 + 2i(\omega_L - \omega_S)\gamma} \quad (10.3.34)$$

so that the total polarization at the Stokes frequency is given by

$$P(\omega_S) = 6\epsilon_0\chi_R(\omega_S)|A_L|^2 A_S e^{ik_S z} + 3\epsilon_0\chi_F(\omega_S)A_L^2 A_a^* e^{i(2k_L - k_a)z}. \quad (10.3.35)$$

This four-wave mixing contribution was not included earlier in Eq. (10.3.16) because we had not included an anti-Stokes field in Eq. (10.3.8). The Stokes four-wave mixing susceptibility is related to the Raman Stokes susceptibility by

$$\chi_F(\omega_S) = 2\chi_R(\omega_S) \quad (10.3.36)$$

and to the anti-Stokes susceptibility through

$$\chi_F(\omega_S) = \chi_F(\omega_a)^*. \quad (10.3.37)$$

The spatial evolution of the Stokes and anti-Stokes fields is now obtained by introducing Eqs. (10.3.33) and (10.3.35) into the driven wave Eq. (2.1.17). We assume that the medium is optically isotropic and that the slowly varying amplitude and constant-pump approximations are valid. We find that the field amplitudes obey the set of coupled equations

$$\frac{dA_S}{dz} = -\alpha_S A_S + \kappa_S A_a^* e^{i\Delta k z}, \quad (10.3.38a)$$

$$\frac{dA_a}{dz} = -\alpha_a A_a + \kappa_a A_S^* e^{i\Delta k z}, \quad (10.3.38b)$$

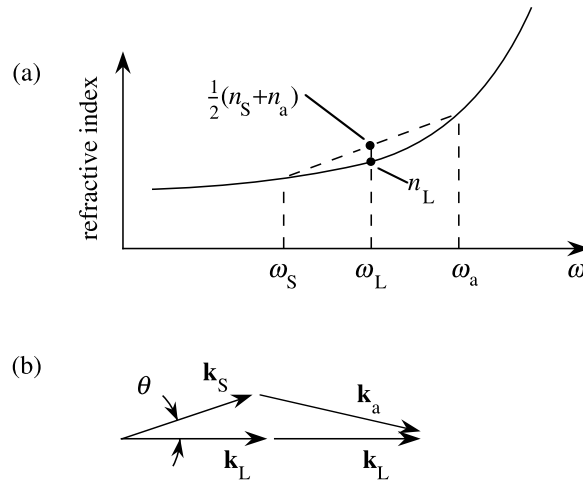


FIGURE 10.3.5: Phase-matching relations for Stokes and anti-Stokes coupling in stimulated Raman scattering.

where we have introduced nonlinear absorption and coupling coefficients

$$\alpha_j = \frac{-3i\omega_j}{n_j c} \chi_R(\omega_j) |A_L|^2, \quad j = S, a, \quad (10.3.39a)$$

$$\kappa_j = \frac{3i\omega_j}{2n_j c} \chi_F(\omega_j) A_L^2, \quad j = S, a, \quad (10.3.39b)$$

and have defined the wavevector mismatch

$$\Delta k = \Delta \mathbf{k} \cdot \hat{\mathbf{z}} = (2\mathbf{k}_L - \mathbf{k}_S - \mathbf{k}_a) \cdot \hat{\mathbf{z}}. \quad (10.3.40)$$

The form of Eqs. (10.3.38) shows that each of the Stokes and anti-Stokes amplitudes is driven by a Raman gain or loss term (the first term on the right-hand side) and by a phase-matched four-wave mixing term (the second). The four-wave mixing term is an effective driving term only when the wavevector mismatch Δk is small. For a material with normal dispersion, the refractive index experienced by the laser wave is always smaller than the mean of those experienced by the Stokes and anti-Stokes waves, as illustrated in part (a) of Fig. 10.3.5. For this reason, perfect phase matching ($\Delta k = 0$) can always be achieved if the Stokes wave propagates at some nonzero angle with respect to the laser wave, as illustrated in part (b) of the figure. For angles appreciably different from this phase-matching angle, Δk is large, and only the first term on the right-hand side of each of Eqs. (10.3.38) is important. For these directions, the two equations decouple, and the Stokes sideband experiences gain and the anti-Stokes sideband experiences loss. However, for directions such that Δk is small, both driving terms on the

right-hand sides of Eqs. (10.3.38) are important, and the two equations must be solved simultaneously. In the next section, we shall see how to solve these equations and shall see that both Stokes and anti-Stokes radiation can be generated in directions for which Δk is small.

10.4 Stokes–Anti-Stokes Coupling in Stimulated Raman Scattering

In this section, we study the nature of the solution to the equations describing the propagation of the Stokes and anti-Stokes waves. We have just seen that these equations are of the form

$$\frac{dA_1}{dz} = -\alpha_1 A_1 + \kappa_1 A_2^* e^{i\Delta kz}, \quad (10.4.1a)$$

$$\frac{dA_2^*}{dz} = -\alpha_2^* A_2^* + \kappa_2^* A_1 e^{-i\Delta kz}. \quad (10.4.1b)$$

In fact, equations of this form are commonly encountered in nonlinear optics and also describe, for example, any forward four-wave mixing process in the constant-pump approximation. The ensuing discussion of the solution to these equations is simplified by first rewriting Eqs. (10.4.1) as

$$e^{-i\Delta kz/2} \left(\frac{dA_1}{dz} + \alpha_1 A_1 \right) = \kappa_1 A_2^* e^{i\Delta kz/2}, \quad (10.4.2a)$$

$$e^{i\Delta kz/2} \left(\frac{dA_2^*}{dz} + \alpha_2^* A_2^* \right) = \kappa_2^* A_1 e^{-i\Delta kz/2}, \quad (10.4.2b)$$

from which it follows that the equations can be expressed as

$$\left(\frac{d}{dz} + \alpha_1 + \frac{i\Delta k}{2} \right) A_1 e^{-i\Delta kz/2} = \kappa_1 A_2^* e^{i\Delta kz/2}, \quad (10.4.3a)$$

$$\left(\frac{d}{dz} + \alpha_2^* - \frac{i\Delta k}{2} \right) A_2^* e^{i\Delta kz/2} = \kappa_2^* A_1 e^{-i\Delta kz/2}. \quad (10.4.3b)$$

The form of these equations suggests that we introduce the new variables F_1 and F_2 defined by

$$F_1 = A_1 e^{-i\Delta kz/2} \quad \text{and} \quad F_2^* = A_2^* e^{i\Delta kz/2}, \quad (10.4.4)$$

so that Eqs. (10.4.3) become

$$\left(\frac{d}{dz} + \alpha_1 + i\frac{\Delta k}{2} \right) F_1 = \kappa_1 F_2^*, \quad (10.4.5a)$$

$$\left(\frac{d}{dz} + \alpha_2^* - i\frac{\Delta k}{2} \right) F_2^* = \kappa_2^* F_1. \quad (10.4.5b)$$

We now eliminate F_2^* algebraically from this set of equations to obtain the single equation

$$\left(\frac{d}{dz} + \alpha_2^* - i\frac{\Delta k}{2}\right)\left(\frac{d}{dz} + \alpha_1 + i\frac{\Delta k}{2}\right)F_1 = \kappa_1\kappa_2^*F_1. \quad (10.4.6)$$

We solve this equation by adopting a trial solution of the form

$$F_1(z) = F_1(0)e^{gz}, \quad (10.4.7)$$

where g represents an unknown spatial growth rate. We substitute this form into Eq. (10.4.6) and find that this equation is satisfied by the trial solution if g satisfies the algebraic equation

$$\left(g + \alpha_2^* - \frac{i\Delta k}{2}\right)\left(g + \alpha_1 + \frac{i\Delta k}{2}\right) = \kappa_1\kappa_2^*. \quad (10.4.8)$$

In general, this equation possesses two solutions, which are given by

$$g_{\pm} = -\frac{1}{2}(\alpha_1 + \alpha_2^*) \pm \frac{1}{2}\left[(\alpha_1 - \alpha_2^* + i\Delta k)^2 + 4\kappa_1\kappa_2^*\right]^{1/2}. \quad (10.4.9)$$

Except for special values of $\alpha_1, \alpha_2, \kappa_1, \kappa_2$, and Δk , the two values of g given by Eq. (10.4.9) are distinct. Whenever the two values of g are distinct, the general solution for F is given by

$$F_1 = F_1^+(0)e^{g_+z} + F_1^-(0)e^{g_-z}, \quad (10.4.10)$$

and thus through the use of Eq. (10.4.4) we see that the general solution for A_1 is of the form

$$A_1(z) = (A_1^+e^{g_+z} + A_1^-e^{g_-z})e^{i\Delta kz/2}. \quad (10.4.11)$$

Here A_1^+ and A_1^- are constants of integration whose values must be determined from the relevant boundary conditions. The general form of the solution for $A_2^*(z)$ is readily found by substituting Eq. (10.4.11) into Eq. (10.4.3a), which becomes

$$\left(g_+ + \alpha_1 + i\frac{\Delta k}{2}\right)A_1^+e^{g_+z} + \left(g_- + \alpha_1 + i\frac{\Delta k}{2}\right)A_1^-e^{g_-z} = \kappa_1A_2^*e^{i\Delta kz/2}.$$

This equation is now solved for $A_2^*(z)$ to obtain

$$A_2^*(z) = \left[\left(\frac{g_+ + \alpha_1 + i\Delta k/2}{\kappa_1}\right)A_1^+e^{g_+z} + \left(\frac{g_- + \alpha_1 + i\Delta k/2}{\kappa_1}\right)A_1^-e^{g_-z}\right]e^{-i\Delta kz/2}. \quad (10.4.12)$$

If we define constants A_2^+ and A_2^- by means of the equation

$$A_2^*(z) = (A_2^{+*}e^{g_+z} + A_2^{-*}e^{g_-z})e^{-i\Delta kz/2}, \quad (10.4.13)$$

we see that the amplitudes A_1^\pm and A_2^\pm are related by

$$\frac{A_2^{\pm*}}{A_1^\pm} = \frac{g_\pm + \alpha_1 + i\Delta k/2}{\kappa_1}. \quad (10.4.14)$$

This equation shows how the amplitudes A_2^+ and A_1^+ are related in the part of the solution that grows as $\exp(g_+z)$, and similarly how the amplitudes A_2^- and A_1^- are related in the part of the solution that grows as $\exp(g_-z)$. We can think of Eq. (10.4.14) as specifying the eigenmodes of propagation of the Stokes and anti-Stokes waves. As written, Eq. (10.4.14) appears to be asymmetric with respect to the roles of the ω_1 and ω_2 fields. However, this asymmetry occurs in appearance only. Since g_\pm depends on $\alpha_1, \alpha_2, \kappa_1, \kappa_2$, and Δk , the right-hand side of Eq. (10.4.14) can be written in a variety of equivalent ways, some of which display the symmetry of the interaction more explicitly. We next rewrite Eq. (10.4.14) in such a manner.

One can show by explicit calculation using Eq. (10.4.9) that the quantities g_+ and g_- are related by

$$\left(g_+ + \alpha_1 + \frac{i\Delta k}{2}\right)\left(g_- + \alpha_1 + \frac{i\Delta k}{2}\right) = -\kappa_1\kappa_2^*. \quad (10.4.15)$$

In addition, one can see by inspection of Eq. (10.4.9) that their difference is given by

$$g_+ - g_- = [(\alpha_1 - \alpha_2^* + i\Delta k)^2 + 4\kappa_1\kappa_2^*]^{1/2}. \quad (10.4.16a)$$

By substitution of Eq. (10.4.9) into this last equation, it follows that

$$g_+ - g_- = \pm[2g_\pm + (\alpha_1 + \alpha_2^*)], \quad (10.4.16b)$$

where on the right-hand side either both pluses or both minuses must be used. Furthermore, one can see from Eq. (10.4.9) that

$$g_+ + g_- = -(\alpha_1 + \alpha_2^*). \quad (10.4.16c)$$

By rearranging this equation and adding $i\Delta k/2$ to each side, it follows that

$$\left(g_\pm + \alpha_1 + \frac{i\Delta k}{2}\right) = -\left(g_\mp + \alpha_2^* - \frac{i\Delta k}{2}\right), \quad (10.4.17a)$$

$$\left(g_\pm + \alpha_2^* + \frac{i\Delta k}{2}\right) = -\left(g_\mp + \alpha_1 + \frac{i\Delta k}{2}\right). \quad (10.4.17b)$$

Through the use of Eqs. (10.4.15) and (10.4.17a), Eq. (10.4.14) can be expressed as

$$\frac{A_2^{\pm*}}{A_1^\pm} = \frac{g_\pm + \alpha_1 + i\Delta k/2}{\kappa_1} = \frac{-\kappa_2^*}{g_\mp + \alpha_1 + i\Delta k/2} = \frac{\kappa_2^*}{g_\pm + \alpha_2^* - i\Delta k/2}. \quad (10.4.18)$$

By taking the geometric mean of the last and third-last forms of this expression, we find that the ratio $A_2^{\pm*}/A_1^{\pm}$ can be written as

$$\frac{A_2^{\pm*}}{A_1^{\pm}} = \left[\frac{\kappa_2^*(g_{\pm} + \alpha_1 + i\Delta k/2)}{\kappa_1(g_{\pm} + \alpha_2^* - i\Delta k/2)} \right]^{1/2}; \quad (10.4.19)$$

this form shows explicitly the symmetry between the roles of the ω_1 and ω_2 fields.

Next, we find the form of the solution when the boundary conditions are such that the input fields are known at the plane $z = 0$ —that is, when $A_1(0)$ and $A_2^*(0)$ are given. We proceed by finding the values of the constants of integration A_1^+ and A_1^- . Eq. (10.4.11) is evaluated at $z = 0$ to give the result

$$A_1(0) = A_1^+ + A_1^-, \quad (10.4.20a)$$

and Eq. (10.4.12) is evaluated at $z = 0$ to give the result

$$A_2^*(0) = \left(\frac{g_+ + \alpha_1 + i\Delta k/2}{\kappa_1} \right) A_1^+ + \left(\frac{g_- + \alpha_1 + i\Delta k/2}{\kappa_1} \right) A_1^-. \quad (10.4.20b)$$

We rearrange Eq. (10.4.20a) to find that $A_1^- = A_1(0) - A_1^+$, and we substitute this form into Eq. (10.4.20b) to obtain

$$A_2^*(0) = \left(\frac{g_+ - g_-}{\kappa_1} \right) A_1^+ + \left(\frac{g_- + \alpha_1 + i\Delta k/2}{\kappa_1} \right) A_1(0).$$

We solve this equation for A_1^+ to obtain

$$A_1^+ = \left(\frac{\kappa_1}{g_+ - g_-} \right) A_2^*(0) - \left(\frac{g_- + \alpha_1 + i\Delta k/2}{g_+ - g_-} \right) A_1(0). \quad (10.4.21a)$$

If instead we solve Eq. (10.4.20a) for A_1^- and substitute the result $A_1^+ = A_1(0) - A_1^-$ into Eq. (10.4.20b), we find that

$$A_2^*(0) = \left(\frac{g_- - g_+}{\kappa_1} \right) A_1^- - \left(\frac{g_+ + \alpha_1 + i\Delta k/2}{\kappa_1} \right) A_1(0),$$

which can be solved for A_1^- to obtain

$$A_1^- = - \left(\frac{\kappa_1}{g_+ - g_-} \right) A_2^*(0) + \left(\frac{g_+ + \alpha_1 + i\Delta k/2}{g_+ - g_-} \right) A_1(0). \quad (10.4.21b)$$

The expressions (10.4.21) for the constants A_1^+ and A_1^- are now substituted into Eqs. (10.4.11) and (10.4.12) to give the solution for the spatial evolution of the two interacting fields in terms

of their boundary values as

$$A_1(z) = \frac{1}{g_+ - g_-} \left\{ \left[\kappa_1 A_2^*(0) - \left(g_- + \alpha_1 + \frac{i \Delta k}{2} \right) A_1(0) \right] e^{g_+ z} - \left[\kappa_1 A_2^*(0) - \left(g_+ + \alpha_1 + \frac{i \Delta k}{2} \right) A_1(0) \right] e^{g_- z} \right\} e^{i \Delta k z / 2} \quad (10.4.22)$$

and

$$A_2^*(z) = \frac{1}{g_+ - g_-} \left\{ \left[\left(g_+ + \alpha_1 + \frac{i \Delta k}{2} \right) A_2^*(0) + \kappa_2^* A_1(0) \right] e^{g_+ z} - \left[\left(g_- + \alpha_1 + \frac{i \Delta k}{2} \right) A_2^*(0) + \kappa_2^* A_1(0) \right] e^{g_- z} \right\} e^{-i \Delta k z / 2}. \quad (10.4.23)$$

Through use of Eqs. (10.4.17), the second form can be written in terms of α_2 instead of α_1 as

$$A_2^*(z) = \frac{1}{g_+ - g_-} \left\{ \left[- \left(g_- + \alpha_2^* - \frac{i \Delta k}{2} \right) A_2^*(0) + \kappa_2^* A_1(0) \right] e^{g_+ z} + \left[\left(g_+ + \alpha_2^* - \frac{i \Delta k}{2} \right) A_2^*(0) - \kappa_2^* A_1(0) \right] e^{g_- z} \right\} e^{-i \Delta k z / 2}. \quad (10.4.24)$$

Before applying the results of the derivation just performed to the case of stimulated Raman scattering, let us make sure that the solution makes sense by applying it to several specific limiting cases.

10.4.1 Dispersionless, Nonlinear Medium without Gain or Loss

For a medium without gain (or loss), we set $\alpha_1 = \alpha_2 = 0$. Also, for a medium that is lossless and dispersionless, $\chi^{(3)}(\omega_1 = 2\omega_0 - \omega_2)$ must equal $\chi^{(3)}(\omega_2 = 2\omega_0 - \omega_1)$, and thus the product $\kappa_1 \kappa_2^*$ that appears in the solution is equal to

$$\kappa_1 \kappa_2^* = \frac{9\omega_1 \omega_2}{4n_1 n_2 c^2} |\chi^{(3)}(\omega_1 = 2\omega_0 - \omega_2)|^2 |A_0|^4, \quad (10.4.25)$$

which is a real, positive quantity. We allow Δk to be arbitrary. Under these conditions, the coupled gain coefficient of Eq. (10.4.9) reduces to

$$g_{\pm} = \pm [\kappa_1 \kappa_2^* - (\Delta k / 2)^2]^{1/2}. \quad (10.4.26)$$

We see that, so long as Δk is not too large, the root g_+ will be a positive real number corresponding to amplification, whereas the root g_- will be a negative real number corresponding to attenuation. However, if the wavevector mismatch becomes so large that Δk^2 exceeds $4\kappa_1 \kappa_2^*$,

both roots will become pure imaginary, indicating that each eigensolution shows oscillatory spatial behavior. According to Eq. (10.4.14), the ratio of amplitudes corresponding to each eigensolution is given by

$$\frac{A_2^{\pm*}}{A_1^{\pm}} = \frac{g_{\pm} + i\Delta k/2}{\kappa_1}. \quad (10.4.27)$$

The right-hand side of this expression simplifies considerably for the case of perfect phase matching ($\Delta k = 0$) and becomes $\pm(\kappa_2^*/\kappa_1)^{1/2}$. If we also choose our phase conventions so that A_0 is purely real, we find that expression reduces to

$$\frac{A_2^{\pm*}}{A_1^{\pm}} = \pm i \left(\frac{n_1 \omega_2}{n_2 \omega_1} \right)^{1/2} \simeq \pm i, \quad (10.4.28)$$

which shows that the two frequency sidebands are phased by $\pm\pi/2$ radians in each of the eigensolutions.

10.4.2 Medium without a Nonlinearity

One would expect on physical grounds that, for a medium in which $\chi^{(3)}$ vanishes, the solution would reduce to the usual case of the free propagation of the ω_1 and ω_2 waves. We now verify that our formal solution possesses this property. By setting $\kappa_1 = \kappa_2 = 0$ in Eq. (10.4.9), and assuming for simplicity that Δk vanishes, we find that

$$g_+ = -\alpha_2^* \quad \text{and} \quad g_- = -\alpha_1. \quad (10.4.29)$$

The eigenamplitudes are found most readily from Eq. (10.4.19). If we assume that κ_1 and κ_2 approach zero in such a manner that κ_2^*/κ_1 remains finite, we find from Eq. (10.4.19) that

$$\frac{A_2^{+*}}{A_1^+} = \infty, \quad \frac{A_2^{-*}}{A_1^-} = 0. \quad (10.4.30)$$

Thus, the positive root corresponds to a wave at frequency ω_2 , which propagates according to

$$A_2^*(z) = A_2^*(0)e^{g_+z} = A_2^*(0)e^{-\alpha_2^*z}, \quad (10.4.31a)$$

whereas the negative root corresponds to a wave at frequency ω_1 , which propagates according to

$$A_1(z) = A_1(0)e^{g_-z} = A_1(0)e^{-\alpha_1z}. \quad (10.4.31b)$$

We thus see that each of the waves simply experiences free propagation.

10.4.3 Stokes–Anti-Stokes Coupling in Stimulated Raman Scattering

Let us now apply this analysis to the case of stimulated Raman scattering (see also Bloembergen and Shen, 1964). For definiteness, we associate ω_1 with the Stokes frequency ω_S and ω_2 with the anti-Stokes frequency ω_a . The nonlinear absorption coefficients α_S and α_a and coupling coefficients κ_S and κ_a are given by Eqs. (10.3.39) with the nonlinear susceptibilities given by Eqs. (10.3.19b), (10.3.25), (10.3.31), and (10.3.34). In light of the relations

$$\chi_F(\omega_S) = \chi_F(\omega_a)^* = 2\chi_R(\omega_S) = 2\chi_R(\omega_a)^* \quad (10.4.32)$$

among the various elements of the susceptibility, we find that the absorption and coupling coefficients can be related to each other as follows:

$$\alpha_a = -\alpha_S^* \left(\frac{n_S \omega_a}{n_a \omega_S} \right), \quad (10.4.33a)$$

$$\kappa_S = -\alpha_S e^{2i\phi_L}, \quad (10.4.33b)$$

$$\kappa_a = \alpha_S^* \left(\frac{n_S \omega_a}{n_a \omega_S} \right) e^{2i\phi_L}, \quad (10.4.33c)$$

where ϕ_L is the phase of the pump laser defined through

$$A_L = |A_L| e^{i\phi_L}, \quad (10.4.34)$$

and where the Stokes amplitude absorption coefficient is given explicitly by

$$\alpha_S = \frac{-i\omega_S N \epsilon_0^2 (\partial\alpha/\partial q)_0^2 |A_L|^2}{4mn_{SC}\omega_v[\omega_S - (\omega_L - \omega_v) + i\gamma]}. \quad (10.4.35)$$

If we now introduce the relations (10.4.33) into the expression (10.4.9) for the coupled gain coefficient, we find the gain eigenvalues are given by

$$g_{\pm} = -\frac{1}{2}\alpha_S \left(1 - \frac{n_S \omega_a}{n_a \omega_S} \right) \pm \frac{1}{2} \left\{ \left[\alpha_S \left(1 + \frac{n_S \omega_a}{n_a \omega_S} \right) + i\Delta k \right]^2 - 4\alpha_S^2 \frac{n_S \omega_a}{n_a \omega_S} \right\}^{1/2}. \quad (10.4.36)$$

It is usually an extremely good approximation to set the factor $n_S \omega_L / n_a \omega_S$ equal to unity. In this case Eq. (10.4.36) simplifies to

$$g_{\pm} = \pm [i\alpha_S \Delta k - (\Delta k/2)^2]^{1/2}. \quad (10.4.37)$$

The dependence of g_{\pm} on the phase mismatch is shown graphically in Fig. 10.4.1.* Eq. (10.4.37) leads to the perhaps surprising result that the coupled gain g_{\pm} vanishes in the limit of perfect phase matching. The reason for this behavior is that, for sufficiently small Δk , the anti-Stokes wave (which normally experiences loss) is so strongly coupled to the Stokes wave (which normally experiences gain) that it prevents the Stokes wave from experiencing growth.

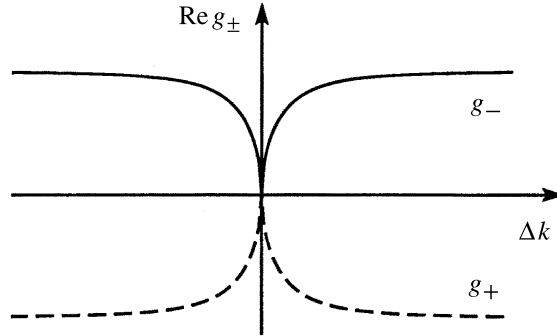


FIGURE 10.4.1: Dependence of the coupled gain on the wavevector mismatch.

It is also instructive to study the expression (10.4.37) for the coupled gain in the limit in which $|\Delta k|$ is very large. For $|\Delta k| \gg |\alpha_S|$, Eq. (10.4.37) becomes

$$g_{\pm} = \pm i \frac{\Delta k}{2} \left(1 - \frac{4i\alpha_S}{\Delta k} \right) \simeq \pm \left(\alpha_S + \frac{1}{2}i\Delta k \right). \quad (10.4.38)$$

Through the use of Eq. (10.4.14), we find that the ratio of sidemode amplitudes associated with each of these gain eigenvalues is given by

$$\frac{A_a^{+*}}{A_S^+} = -2 - i \frac{\Delta k}{\alpha_S} \simeq i \frac{\Delta k}{\alpha_S}, \quad (10.4.39a)$$

$$\frac{A_a^{-*}}{A_S^-} = 0. \quad (10.4.39b)$$

Since we have assumed that $|\Delta k|$ is much larger than $|\alpha_S|$, we see that the $+$ mode is primarily anti-Stokes, whereas the $-$ mode is primarily Stokes.[†]

Let us now examine more carefully the nature of the decreased gain that occurs near $\Delta k = 0$. By setting $\Delta k = 0$ in the exact expression (10.4.36) for the coupled gain, we find that the gain

* The graph has the same visual appearance whether the approximate form (10.4.37) or the exact form (10.4.36) is plotted.

† Recall that at resonance α_S is real and *negative*; hence $g_- = -\alpha_S - \frac{1}{2}i\Delta k$ has a positive real part and leads to amplification.

eigenvalues become

$$g_+ = 0, \quad g_- = -\alpha_S \left(1 - \frac{n_S \omega_a}{n_a \omega_S} \right). \quad (10.4.40)$$

Note that $|g_-|$ is much smaller than $|\alpha_S|$ but does not vanish identically. Note also that with the sign convention used here at resonance g_- is a negative quantity. We find from Eq. (10.4.14) that for a good approximation

$$\frac{A_a^{\pm*}}{A_S^{\pm}} = -1; \quad (10.4.41)$$

thus, each eigensolution is seen to be an equal combination of Stokes and anti-Stokes components, as mentioned in our discussion of Fig. 10.4.1.

Next, let us consider the spatial evolution of the field amplitudes under the assumptions that $\Delta k = 0$ and that their values are known at $z = 0$. We find from Eqs. (10.4.22) and (10.4.23) that

$$A_S(z) = \frac{-1}{1 - n_S \omega_a / n_a \omega_S} \left\{ \left[A_a^*(0) e^{2i\phi_L} + \frac{n_S \omega_a}{n_a \omega_S} A_S(0) \right] - \left[A_a^*(0) e^{2i\phi_L} + A_S(0) \right] e^{g_- z} \right\}, \quad (10.4.42a)$$

$$A_a^*(z) = \frac{1}{1 - n_S \omega_a / n_a \omega_S} \left\{ \left[A_a^*(0) + \frac{n_S \omega_a}{n_a \omega_S} A_S(0) e^{-2i\phi_L} \right] - \frac{n_S \omega_a}{n_a \omega_S} \left[A_a^*(0) + A_S(0) e^{-2i\phi_L} \right] e^{g_- z} \right\}. \quad (10.4.42b)$$

Note that, since g_- is negative, the second term in each expression experiences exponential decay, and as $z \rightarrow \infty$ the field amplitudes approach the asymptotic values

$$A_S(z \rightarrow \infty) = \frac{-1}{1 - n_S \omega_a / n_a \omega_S} \left[A_a^*(0) e^{2i\phi_L} + \frac{n_S \omega_a}{n_a \omega_S} A_S(0) \right], \quad (10.4.43a)$$

$$A_a^*(z \rightarrow \infty) = \frac{1}{1 - n_S \omega_a / n_a \omega_S} \left[A_a^*(0) + \frac{n_S \omega_a}{n_a \omega_S} A_S(0) e^{-2i\phi_L} \right]. \quad (10.4.43b)$$

Note that each field is amplified by the factor $(1 - n_S \omega_a / n_a \omega_S)^{-1}$. The nature of this amplification is illustrated in part (a) of Fig. 10.4.2. We see that after propagating through a distance of several times $1/g_-$, the field amplitudes attain constant values and no longer change with propagation distance.

To see why field amplitudes remain constant, it is instructive to consider the nature of the molecule vibration in the simultaneous presence of the laser, Stokes, and anti-Stokes fields—that is, in the field

$$\tilde{E}(z, t) = A_L e^{i(k_L z - \omega_L t)} + A_S e^{i(k_S z - \omega_S t)} + A_a e^{i(k_a z - \omega_a t)} + \text{c.c.}, \quad (10.4.44)$$

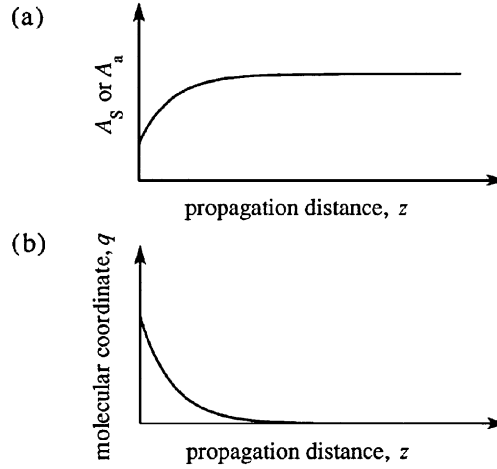


FIGURE 10.4.2: Nature of Raman amplification for the case of perfect phase matching ($\Delta k = 0$).

where $k_L - k_S = k_a - k_L \equiv K$ and $\omega_L - \omega_S = \omega_a - \omega_L \equiv \Omega$. The solution to the equation of motion (10.3.1) for the molecular vibration with the force term given by Eqs. (10.3.6) and (10.4.44) is given by

$$\tilde{q}(z, t) = q(\Omega)e^{i(Kz - \Omega t)} + \text{c.c.},$$

where

$$g(\Omega) = \frac{(\epsilon_0/m)(\partial\alpha/\partial q)_0(A_L A_S^* + A_a A_L^*)}{\omega_v^2 - \Omega^2 - 2i\Omega\gamma}. \quad (10.4.45)$$

We can see from Eqs. (10.4.43) that, once the field amplitudes have attained their asymptotic values, the combination $A_L A_S^* + A_a A_L^*$ vanishes, implying that the amplitude $q(\omega)$ of the molecular vibration also vanishes asymptotically, as illustrated in part (b) of Fig. 10.4.2.

10.5 Coherent Anti-Stokes Raman Scattering

In the previous sections of this chapter, we discussed spontaneous Raman scattering and stimulated Raman scattering. These processes are represented symbolically in parts (a) and (b) of Fig. 10.5.1. In the notation of Section 10.3, stimulated Raman scattering is described by a nonlinear susceptibility of the form $\chi_R^{(3)}(\omega_S = \omega_S + \omega_L - \omega_L)$. We also saw in that section (see, for example, Eqs. (10.3.20) and (10.3.21)) that the Stokes wave at frequency ω_S tends to experience exponential growth, with a growth rate that scales as the product of the laser intensity and the imaginary part of $\chi_R^{(3)}$.

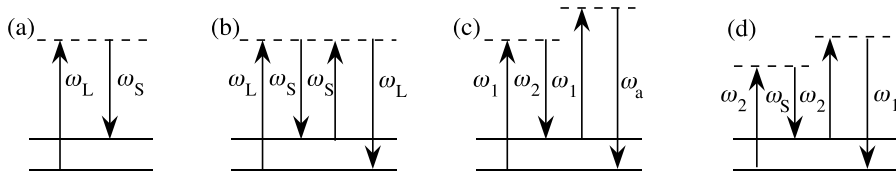


FIGURE 10.5.1: Various Raman scattering processes: (a) spontaneous Raman scattering; (b) stimulated Raman scattering; (c) coherent anti-Stokes Raman scattering (CARS); and (d) coherent Stokes Raman scattering (CSRS).

In the present section, we study two additional scattering processes, also shown in Fig. 10.5.1, known as coherent anti-Stokes Raman scattering (CARS) and coherent Stokes Raman scattering (CSRS). Our discussion will concentrate on the first of these processes, as it is the one most often used in laboratory investigations. In either of these processes, two laser beams at frequencies ω_1 and $\omega_2 < \omega_1$ are applied to the Raman medium, and a beam at a new frequency is generated by the interaction. In the process of coherent anti-Stokes Raman scattering (CARS), illustrated in part (c) of the figure, an output is created at frequency $2\omega_1 - \omega_2$ as a consequence of the susceptibility $\chi_F^{(3)}(\omega_a = \omega_1 - \omega_2 + \omega_1)$. In the process of coherent Stokes Raman scattering (CSRS), illustrated in part (d) of the figure, an output is created at frequency $2\omega_2 - \omega_1$ as a consequence of the susceptibility $\chi_F^{(3)}(\omega_s = \omega_2 + \omega_2 - \omega_1)$.

Let us now analyze more carefully the process of coherent anti-Stokes Raman scattering (CARS). We recall from Section 10.3 that the susceptibility describing this process is given according to Eqs. (10.3.25) and (10.3.32) for the current choice of frequencies by

$$\chi_F^{(3)}(\omega_a = \omega_1 - \omega_2 + \omega_1) = \frac{-(\epsilon_0 N / 6m\omega_v)(\partial\alpha/\partial q)_0^2}{[(\omega_1 - \omega_2) - \omega_v] + i\gamma}. \quad (10.5.1)$$

Note that the nonlinear response experiences a resonance whenever the input frequencies ω_1 and ω_2 are selected so that $\omega_1 - \omega_2$ is equal to a vibrational frequency ω_v of the material system. It is for this reason that CARS is particularly useful as a diagnostic tool for determining the presence of chemical species by means of their Raman vibrational modes. CARS is also useful as a probe of molecular structure because the resonance frequency ω_v and relaxation rate γ often depend sensitively upon the molecular environment.

The generation of the anti-Stokes wave is described by the coupled-amplitude equation Eq. (10.3.38b), which for the current situation becomes

$$\frac{dA_a}{dz} = -\alpha_a A_a + \kappa_a A_2^* e^{i\Delta kz}, \quad (10.5.2)$$

where

$$\alpha_a = \frac{-3i\omega_a}{n_a c} \chi_R(\omega_a) |A_1|^2, \quad \kappa_a = \frac{3i\omega_a}{2n_a c} \chi_F(\omega_a) A_1^2, \quad (10.5.3)$$

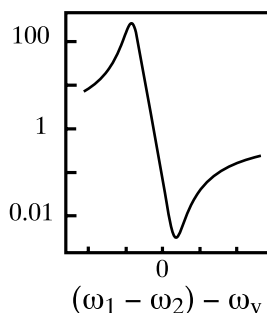


FIGURE 10.5.2: Typical CARS lineshape, such as that reported by Levenson and Bloembergen (1974).

and

$$\Delta k = \Delta \mathbf{k} \cdot \hat{\mathbf{z}} = (2\mathbf{k}_1 - \mathbf{k}_2 - \mathbf{k}_a) \cdot \hat{\mathbf{z}}. \quad (10.5.4)$$

CARS is usually studied under conditions such that the generation of the anti-Stokes signal is dominated by the second term on the right-hand side of Eq. (10.5.2). This situation occurs whenever the gain of stimulated Raman scattering (described by the first term) is small. Under this assumption and that of perfect phase matching ($\Delta k = 0$), the growth of the anti-Stokes wave can be expressed as

$$A_a(z) = \frac{3i\omega_a}{2n_a c} \chi_F(\omega_a) A_1^2 A_2^* z. \quad (10.5.5)$$

The spectral variation of the anti-Stokes generation as either of the two input frequencies is varied is determined by $|\chi_F(\omega_a)|^2$, and thus is expected to have a shape in the form of the square of a Lorentzian function. However, it is found experimentally that the measured line shape is often highly distorted. An example of such a line shape is shown in Fig. 10.5.2. The explanation for this behavior is that in addition to the highly resonant molecular response described by Eq. (10.5.1) actual materials also exhibit a nonresonant background susceptibility $\chi_{\text{NR}}^{(3)}$ due to electronic response and to nonresonant vibrational modes. The total susceptibility is then given by $\chi_{\text{NR}}^{(3)} + \chi_F^{(3)}(\omega_a)$, and consequently the lineshape will be given by $|\chi_{\text{NR}}^{(3)} + \chi_F^{(3)}(\omega_a)|^2$, which leads to a line shape of the sort shown in the figure.

The CARS effect was first observed experimentally by Maker and Terhune (1965). Significant early studies were those of Levenson et al. (1972) and Levenson and Bloembergen (1974). The subject of Raman spectroscopy is covered well in the book by Levenson and Kano (1988). The use of CARS for imaging and for microscopy has been reviewed by Volkmer (2005).

10.6 Stimulated Rayleigh-Wing Scattering

Stimulated Rayleigh-wing scattering is the light-scattering process that results from the tendency of anisotropic molecules to become aligned along the electric field vector of an optical wave. Stimulated Rayleigh-wing scattering was described theoretically by Bloembergen and Lallemand (1966) and by Chiao et al. (1966), and was observed experimentally by Mash et al. (1965) and Cho et al. (1967). Other early studies were conducted by Denariez and Bret (1968) and by Foltz et al. (1968).

The molecular orientation effect was described in Section 4.4 for the case in which the applied optical field $\tilde{E}(t)$ contains a single frequency component, and it was found that the average molecular polarizability is modified by the presence of the applied field. The molecular polarizability can be expressed as

$$\langle \alpha \rangle = \alpha_0 + \alpha_{\text{NL}}, \quad (10.6.1)$$

where the usual, weak-field polarizability is given by

$$\alpha_0 = \frac{1}{3}\alpha_{\parallel} + \frac{2}{3}\alpha_{\perp}, \quad (10.6.2)$$

where α_{\parallel} and α_{\perp} denote the polarizabilities measured parallel to the perpendicular to the symmetry axis of the molecule, respectively (see Fig. 10.6.1). In addition, the lowest-order nonlinear contribution to the polarizability is given by

$$\alpha_{\text{NL}} = \bar{\alpha}_2 \langle \tilde{E}^2 \rangle, \quad (10.6.3)$$

where

$$\bar{\alpha}_2 = \frac{2}{45n_0} \frac{(\alpha_{\parallel} - \alpha_{\perp})^2}{kT}. \quad (10.6.4)$$

In order to describe stimulated Rayleigh-wing scattering, we need to determine the response of the molecular system to an optical field that contains both laser and Stokes components, which we describe by the equation

$$\tilde{E}(\mathbf{r}, t) = A_L e^{i(k_L z - \omega_L t)} + A_S e^{i(-k_S z - \omega_S t)} + \text{c.c.} \quad (10.6.5)$$

For the present, we assume that the laser and Stokes waves have the same linear polarization and are counterpropagating. The analysis for the case in which the waves have arbitrary polarization and/or are copropagating is somewhat more involved and is discussed briefly below.

Since the intensity, which is proportional to $\langle \tilde{E}^2 \rangle$, now contains a component at the beat frequency $\omega_L - \omega_S$, the nonlinear contribution to the mean polarizability $\langle \alpha \rangle$ is no longer given

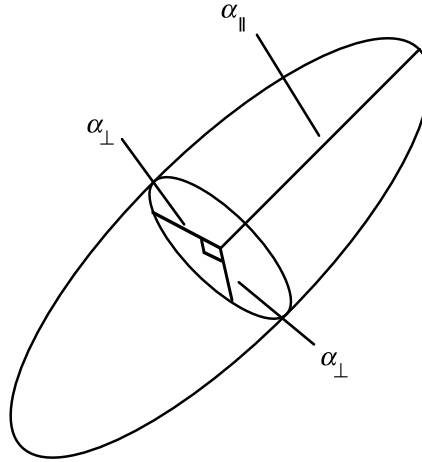


FIGURE 10.6.1: Illustration of the polarizabilities of an anisotropic molecule for the case $\alpha_{\parallel} > \alpha_{\perp}$.

TABLE 10.6.1: Properties of SRWS for several materials.

Substance	G (m/TW)	τ (psec)	$\Delta\nu = 1/2\pi\tau$ (GHz)
CS ₂	30	2	80
Nitrobenzene	30	48	3.3
Bromobenzene	14	15	10
Chlorobenzene	10	8	20
Toluene	10	2	80
Benzene	6	3	53

by Eq. (10.6.3), which was derived for the case of a monochromatic field. We assume that, in general, α_{NL} is described by the equation

$$\tau \frac{d\alpha_{\text{NL}}}{dt} + \alpha_{\text{NL}} = \bar{\alpha}_2 \bar{E}^2. \quad (10.6.6)$$

In this equation τ represents the molecular orientation relaxation time and is the characteristic response time of the SRWS process; see Table 10.6.1 for typical values of τ . Eq. (10.6.6) has the form of a Debye relaxation equation; recall that we have studied equations of this sort in our general discussion of two-beam coupling in Section 7.4.

If Eq. (10.6.6) is solved in steady state with $\bar{E}(t)$ given by Eq. (10.6.5), we find that the nonlinear contribution to the polarizability of a molecule located at position z is given by

$$\alpha_{\text{NL}}(z, t) = 2\bar{\alpha}_2 (A_L A_L^* + A_S A_S^*) + \left(\frac{2\bar{\alpha}_2 A_L A_S^* e^{iqz - \Omega t}}{1 - i\Omega\tau} \right) + \text{c.c.}, \quad (10.6.7)$$

where we have introduced the wavevector magnitude q and frequency Ω associated with the material excitation, which are given by

$$q = k_L + k_S \quad \text{and} \quad \Omega = \omega_L - \omega_S. \quad (10.6.8)$$

Note that because the denominator of the second term in the expression for $\alpha_{\text{NL}}(z, t)$ is a complex quantity, the nonlinear response will in general be shifted in phase with respect to the intensity distribution associated with the interference of the laser and Stokes fields. We shall see below that this phase shift is the origin of the gain of the stimulated Rayleigh-wing scattering process.

We next derive the equation describing the propagation of the Stokes field. This derivation is formally identical to that presented in Section 7.4 in our general discussion of two-beam coupling. To apply that treatment to the present case, we need to determine the values of the refractive indices n_0 and n_2 that are relevant to the problem at hand. We find that n_0 is obtained from the usual Lorentz–Lorenz law (see also Eq. (3.9.8a)) as

$$\frac{n_0^2 - 1}{n_0^2 + 2} = \frac{1}{3} N \alpha_0 \quad (10.6.9a)$$

and that the nonlinear refractive index is given (see also Eqs. (4.1.18) and (4.4.26)) by

$$n_2 = \left(\frac{n_0^2 + 2}{3} \right)^4 \frac{1}{2n_0^2 \epsilon_0 c} N \bar{\alpha}_2. \quad (10.6.9b)$$

Then, as in Eq. (7.4.15), we find that the spatial evolution of the Stokes wave is described by

$$\frac{dA_S}{dz} = \frac{2in_0n_2\omega_S}{c} (A_L A_L^* + A_S A_S^*) A_S + \frac{2in_0n_2\omega_S}{c} \frac{A_L A_L^* A_S}{1 + i\Omega\tau}. \quad (10.6.10)$$

Here the first term on the right-hand side leads to a spatial variation of the phase of the Stokes, whereas the second term leads to both a phase variation and to amplification of the Stokes wave. The gain associated with stimulated Rayleigh-wing scattering can be seen more clearly in terms of the equation relating the intensities of the two waves, which are defined by

$$I_j = 2n_0\epsilon_0 c |A_j|^2, \quad j = L, S. \quad (10.6.11)$$

The spatial variation of the intensity of the Stokes wave is therefore described by

$$\frac{dI_S}{dz} = 2n_0\epsilon_0 c \left[A_S \frac{dA_S^*}{dz} + A_S^* \frac{dA_S}{dz} \right]. \quad (10.6.12)$$

Through use of Eq. (10.6.10), we can write this result as

$$\frac{dI_S}{dz} = g_{RW} I_L I_S, \quad (10.6.13)$$

where we have introduced the gain factor g_{RW} for stimulated Rayleigh-wing scattering, which is given by

$$g_{RW} = g_{RW}^{(\max)} \left(\frac{2\Omega\tau}{1 + \Omega^2\tau^2} \right), \quad (10.6.14a)$$

where $g_{RW}^{(\max)}$ denotes the maximum value of the gain factor, which is given by

$$g_{RW}^{(\max)} = \frac{n_2\omega_S}{c} = \left(\frac{n_0^2 + 2}{3} \right)^4 \frac{2\omega_S N (\alpha_{\parallel} - \alpha_{\perp})^2}{45kT n_0^2 \epsilon_0 c^2}. \quad (10.6.14b)$$

We have made use of Eqs. (10.6.4) and (10.6.9b) in obtaining the second form of the expression for $g_{RW}^{(\max)}$.

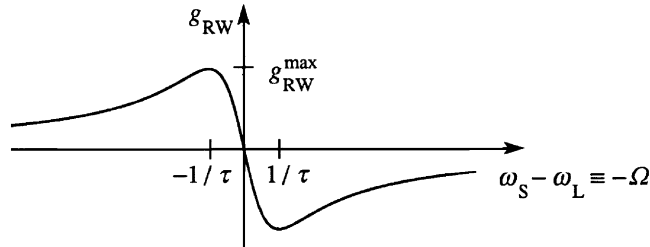


FIGURE 10.6.2: Frequency dependence of the gain factor for stimulated Rayleigh-wing scattering.

The frequency dependence of the gain factor for stimulated Rayleigh-wing scattering as predicted by Eq. (10.6.14a) is illustrated in Fig. 10.6.2. We see that amplification of the ω_S wave occurs for $\omega_S < \omega_L$ and that attenuation occurs for $\omega_S > \omega_L$. The maximum gain occurs when $\Omega \equiv \omega_L - \omega_S$ is equal to $1/\tau$.

The nature of the stimulated Rayleigh-wing scattering process is illustrated schematically in Fig. 10.6.3. The interference of the forward-going wave of frequency ω_L and wavevector magnitude k_L and the backward-going wave of frequency ω_S and wavevector magnitude k_S produces a fringe pattern that moves slowly through the medium in the forward direction with phase velocity $v = \Omega/q$. The tendency of the molecules to become aligned along the electric field vector of the total optical wave leads to planes of maximum molecular alignment alternating with planes of minimum molecular alignment. As mentioned above, these planes are shifted in phase with respect to the maxima and minima of the intensity distributions. The scattering of the laser field from this periodic array of aligned molecules leads to the generation of

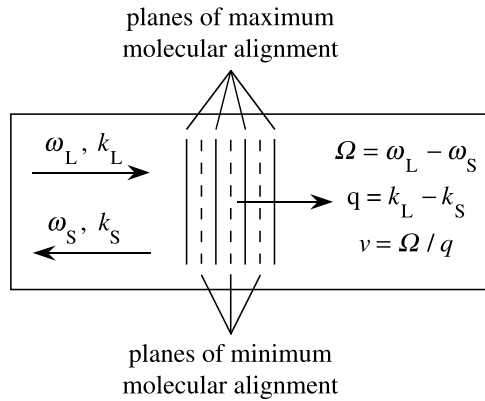


FIGURE 10.6.3: Nature of stimulated Rayleigh-wing scattering.

the Stokes wave. The scattered radiation is shifted to lower frequencies because the material disturbance causing the scattering is moving in the forward direction. The scattering process shows gain because the generation of Stokes radiation tends to reinforce the modulated portion of the interference pattern, which leads to increased molecular alignment and thus to increased scattering of Stokes radiation.

10.6.1 Polarization Properties of Stimulated Rayleigh-Wing Scattering

A theoretical analysis of the polarization properties of stimulated Rayleigh-wing scattering has been conducted by Chiao and Godine. The details of their analysis are quite complicated; here we shall simply quote some of their principal results.

In order to treat the polarization properties of stimulated Rayleigh-wing scattering, one must consider the tensor properties of the material response. The analysis of Chiao and Godine presupposes that the nonlinear contribution to the susceptibility obeys the equation of motion









$$\tau \frac{d}{dt} \Delta \chi_{ik} + \Delta \chi_{ik} = C \left(\langle \tilde{E}_i \tilde{E}_k \rangle - \frac{1}{3} \delta_{ik} \langle \tilde{\mathbf{E}} \cdot \tilde{\mathbf{E}} \rangle \right), \quad (10.6.15)$$

where, ignoring for the present local-field corrections, the proportionality constant C is given by

$$C = \frac{N \epsilon_0^2 (\alpha_{\parallel} - \alpha_{\perp})^2}{15 k T}. \quad (10.6.16)$$







Note that the trace of the right-hand side of Eq. (10.6.15) vanishes, as required by the fact that Rayleigh-wing scattering is described by a traceless, symmetric permittivity tensor.

TABLE 10.6.2: Dependence of the gain factor for stimulated Rayleigh-wing scattering in the backward direction on the polarization of the laser and Stokes waves for the cases of linear and circular polarization^a.

Laser polarization				
Stokes polarization				
Gain factor	1	3/4	3/2	1/6

^a The arrows on the circles denote the direction in which the electric field vector rotates in time at a fixed position in space. The gain factors are given relative to that given by Eqs. (10.6.14) for the case of linear and parallel polarization.

TABLE 10.6.3: Relation between laser polarization and the Stokes polarization experiencing maximum gain in backward stimulated Rayleigh-wing scattering.

Laser			
Stokes			

By requiring that the Stokes wave obey the wave equation with a susceptibility given by the solution to Eq. (10.6.15), and taking account of rotation of the pump laser polarization (see, for example, the discussion in Section 4.2), Chiao and Godine calculate the gain factor for stimulated Rayleigh-wing scattering for arbitrary polarization of the laser and Stokes fields. Some of their results for special polarization cases are summarized in Table 10.6.2.

For any state of polarization of the pump wave, some particular polarization of the Stokes wave will experience maximum gain. As a consequence of the large value of the gain required to observe stimulated light scattering ($g_{RW} I_L L \simeq 25$), the light generated by stimulated Rayleigh-wing scattering will have a polarization that is nearly equal to that for which the gain is maximum. The relation between the laser polarization and the Stokes polarization for which the gain is maximum is illustrated in Table 10.6.3. Note that the generated wave will be nearly, but not exactly, the polarization conjugate (in the sense of vector phase conjugation, as discussed in Section 7.2) of the incident laser wave. In particular, the polarization ellipse of the generated wave will be rounder and tilted with respect to that of the laser wave.

Zel'dovich and Yakovleva (1980) have studied theoretically the polarization properties of stimulated Rayleigh-wing scattering for the case in which the pump radiation is partially polarized. They predict that essentially perfect vector phase conjugation can be obtained by stimulated Rayleigh-wing scattering for the case in which the pump radiation is completely depolarized in the sense that the state of polarization varies randomly over the transverse dimensions of the laser beam. The wavefront-reconstructing properties of stimulated Rayleigh-wing scattering have been studied experimentally by Kudriavtseva et al. (1978), and the vector phase conjugation properties have been studied experimentally by Miller et al. (1990).

The analysis of stimulated Rayleigh-wing scattering in the forward and near-forward direction is much more complicated than that of backward stimulated Rayleigh-wing scattering because the possibility of Stokes–anti-Stokes coupling (as described in Section 10.4 for stimulated Raman scattering) must be included in the analysis. This situation has been described by Chiao et al. (1966) and by Chiao and Godine (1969).

Problems

1. *Estimation of the properties of stimulated Raman scattering.* By making reasonable assumptions regarding the value of the parameter ($d\alpha/dq$), perform an order-of-magnitude estimate of the gain factor for stimulated Raman scattering for condensed matter, and compare this value with the measured values given in Table 10.2.1.
2. *Polarization properties of stimulated Rayleigh-wing scattering.* By carrying out the prescription described in the first full paragraph following Eq. (10.6.16), verify that the entries in Table 10.6.2 are correct.

References

Stimulated Raman Scattering

- Bloembergen, N., 1967. Am. J. Phys. 35, 989.
 Bloembergen, N., Shen, Y.R., 1964. Phys. Rev. Lett. 12, 504.
 Boyd, R.W., 1983. Radiometry and the Detection of Optical Radiation. Wiley, New York.
 Eckhardt, G., Hellwarth, R.W., McClung, F.J., Schwarz, S.E., Weiner, D., Woodbury, E.J., 1962. Phys. Rev. Lett. 9.
 Garmire, E., Pandarese, F., Townes, C.H., 1963. Phys. Rev. Lett. 11, 160.
 Hellwarth, R.W., 1963. Phys. Rev. 130, 1850.
 Kaiser, W., Maier, M., 1972. In: Arecchi, F.T., Schulz-DuBois, E.O. (Eds.), Laser Handbook. North-Holland.
 Penzkofer, A., Laubereau, A., Kaiser, W., 1979. Prog. Quantum Electron. 6, 55.
 Raymer, M.G., Mostowski, J., 1981. Phys. Rev. A 24, 1980.
 Raymer, M.G., Walmsley, I.A., 1990. In: Wolf, E. (Ed.), Progress in Optics, vol. 28. North-Holland, Amsterdam.
 Shen, Y.R., Bloembergen, N., 1965. Phys. Rev. 137, 1787.
 Simon, U., Tittel, F.K., 1994. In: Hulet, R.G., Dunning, F.B. (Eds.), Methods of Experimental Physics, vol. III. Academic Press, San Diego.
 Terhune, R.W., 1963. Bull. Am. Phys. Soc. 8, 359.
 Woodbury, E.J., Ng, W.K., 1962. Proc. IRE 50, 2367.

Tensor Properties of Stimulated Raman Scattering

- Happer, W., 1972. *Rev. Mod. Phys.* 44, 169.
Holmes, R., Flusberg, A., 1988. *Phys. Rev. A* 37, 1588.
Landau, L.D., Lifshitz, E.M., 1960. *Electrodynamics of Continuous Media*. Pergamon Press, Oxford, pp. 377–383.
Pritchett, T., Smith, J., McIntyre, G., Moore, T.R., Oldaker, B.G., 1999. *J. Mod. Opt.* 46, 949.
Venkin, G.V., Ilinskii, Yu A., Mikheev, G.M., 1985. *Kvantovaya Elektron. (Moscow)* 12, 608; *Sov. J. Quantum Electron.* 15, 1985 395.

Coherent Anti-Stokes Raman Scattering

- Levenson, M.D., Bloembergen, N., 1974. *Phys. Rev. B* 10, 4447.
Levenson, M.D., Kano, S.S., 1988. *Introduction of Nonlinear Laser Spectroscopy*. Academic Press, Boston.
Levenson, M.D., Flytzanis, C., Bloembergen, N., 1972. *Phys. Rev. B* 6, 3962.
Maker, P.D., Terhune, R.W., 1965. *Phys. Rev.* 137, A801.
Volkmer, A., 2005. *J. Phys. D* 38, R59.

Stimulated Rayleigh-Wing Scattering

- Bloembergen, N., Lallemand, P., 1966. *Phys. Rev. Lett.* 16, 81.
Chiao, R.Y., Godine, J., 1969. *Phys. Rev.* 185, 430.
Chiao, R.Y., Kelley, P.L., Garmire, E., 1966. *Phys. Rev. Lett.* 17, 1158.
Cho, C.W., Foltz, N.D., Rank, D.H., Wiggins, T.A., 1967. *Phys. Rev. Lett.* 18, 107.
Denariez, M., Bret, G., 1968. *Phys. Rev.* 177, 171.
Foltz, N.D., Cho, C.W., Rank, D.H., Wiggins, T.A., 1968. *Phys. Rev.* 165, 396.
Kudriavtseva, A.D., Sokolovskaia, A.I., Gazengel, J., Phu Xuan, N., Rivore, G., 1978. *Opt. Commun.* 26, 446.
Mash, D.I., Morozov, V.V., Starunov, V.S., Fabelinskii, I.L., 1965. *JETP Lett.* 2, 25.
Miller, E.J., Malcuit, M.S., Boyd, R.W., 1990. *Opt. Lett.* 15, 1189.
Zel'dovich, B.Ya., Yakovleva, T.V., 1980. *Sov. J. Quantum Electron.* 10, 501.